POAC '99
Espoo, Finland

Proceedings of the 15th
International Conference on
Port and Ocean Engineering
under Arctic Conditions

THE USE OF ICE TANK EXPERIMENT RESULTS FOR MESOSCALE SEA ICE MODELLING

Sergei Ovsienko[1], Matti Leppäranta[2], Sergei Zatsepa[1] and Alexander Ivchenko[1]
[1] State Oceanographic Institute, Moscow, Russia
[2] Department of Geophysics, University of Helsinki, Helsinki, Finland

ABSTRACT

Ice tank experiments on ridging and rafting of a granular ice field are examined using a continuum mesoscale sea ice model. The main validation data from these experiments is the force on a pushing plate under compressive deformation. A mathematical elastic-plastic ice model reproduced reasonably well the force history. Both the tank tests and the model outcome show rate-independent plastic behavior in a wide range of velocities. In places the force was underestimated which was likely due to an inappropriate ridging function approximation.

1. INTRODUCTION

In sea ice dynamics the sea ice material - drift ice - is a granular, compressible and nonlinear medium. The mechanical behavior of drift ice is described by semi-empirical rheologies and by a thickness distribution function, and a continuum approximation is commonly taken in modeling applications. Model development and verification has been made with full scale field data. One could think of also physical models or ice tank experiments to provide an additional method to analyze drift ice models. However, such work has not yet been realized.

An extensive series of ice tank experiments on ridging and rafting has been performed by the Arctic Marine Laboratory of the Helsinki University of Technology (HUT) in 1996-1998 (Tuhkuri and Lensu, 1997). The purpose was to examine ridging and rafting processes on a local scale by uniaxial compression of a granular ice field using a pusher plate on one boundary of the ice field. These data seem to be promising also for understanding mesoscale sea ice modeling.

The present paper describes a set of calculations with a continuum mesoscale ice dynamics model applied for the HUT tank tests. The purpose was to adapt such model for ice tank experiments and to evaluate the feasibility of this technique to examine sea ice dynamics and scaling of ice tank outcome into natural scales. A special numerical technique for two-dimensional problems for compressible media with free boundaries is used. The technique is flexible and allows for implementations of different rheologies, while in this calculation an elastic-plastic rheology was used. A moving rigid boundary was introduced to represent the pusher plate in the ice tank experiment conditions.

2. THE DRIFT ICE MODELING PROBLEM

2.1 Mathematical Model

Ice conditions are represented by a thickness distribution $G = G(\boldsymbol{r}, h, t)$ where $\boldsymbol{r}$ is the spatial location, h is ice thickness, and t is time (Thorndike et al., 1975). $G(\boldsymbol{r}, h, t)$ equals the probability that the thickness of ice is h or less in an area at point $\boldsymbol{r}$ and time t. In particular, the compactness of ice is $A(\boldsymbol{r}, t) = G(\boldsymbol{r}, 0, t)$. In the absence of thermodynamics the thickness distribution changes only mechanically due to advection and compaction:

$$DG/Dt + G\,\nabla \cdot \boldsymbol{u} = \psi \qquad (1)$$

where D/Dt is the substantial derivative, ψ is a redistribution function that describes mechanical conversion of ice between categories when rafting and ridging occur, and $\boldsymbol{u}$ is ice velocity.

The function ψ depends on the thickness distribution G and plastic stretching $\boldsymbol{D}_p$ (Thorndike et al., 1975; Pritchard, 1981). Ridging and opening are specified by the ratio of shear to dilatation, and a ridging function W_r tells how ice thickness categories change in ridging. The model behavior is highly dependent on the choice of the ridging function. The main hypotheses introduced by Thorndike et al. (1975) are that (1) ridged ice thickness is k times the original ice thickness and (2) thinner ice is ridged more intensively. It is also assumed that ridged and undeformed ice have the same properties. These hypotheses are taken also here. The ridging function W_r is

$$W_r(h) = \{\int_o^h [n(h_2) - a(h_2)]\mathrm{d}h_2\}/W_r(\infty) \qquad (2)$$

where $n(h_2) = \int_o^\infty \gamma(h_1, h_2) \times a(h_1)\mathrm{d}h_1$ is the fractional area of ice of thickness h_2 produced from ice of original thickness h_1 involved in the ridging process, and the factor $W_r(\infty)$ normalizes for the conservation of ice volume. The assumption (1) above implies that $\gamma(h_1, h_2) = \delta(h_2 - kh_1)/k$; the assumption (2) is embedded in the function a defining the ice fraction participating in the ridging process: $a(h) = b[G(h)]g(h)$ where $g(h) = \mathrm{d}G/\mathrm{d}h$ is the spatial density of ice thickness and $b(G)$ is a shape function describing the availability of ice for ridging (Fig. 1).

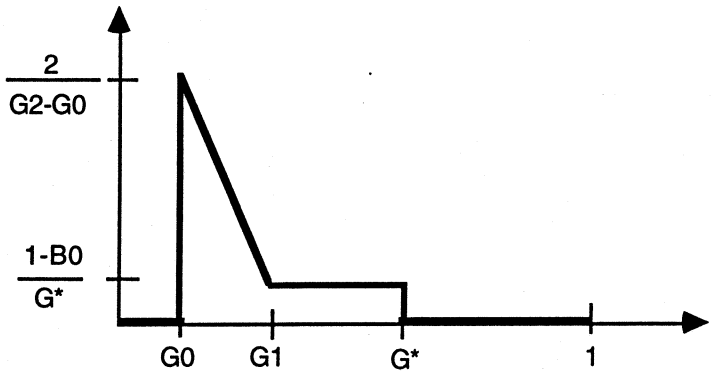

Fig. 1. The shape function b[G(h)] describing the availability of ice for ridging.

The equation of motion of drift ice is (e.g., Hibler, 1979):

$$m(\mathrm{D}\boldsymbol{u}/\mathrm{D}t + f\mathbf{k} \times \boldsymbol{u}) = A(\tau_a + \tau_w) + \nabla \cdot \sigma - mg\nabla\eta \qquad (3)$$

where $m = \rho_i H$, ρ_i is ice density, H is mean ice thickness, f is Coriolis parameter, $\mathbf{k}$ is unit vector vertically upward, τ_a and τ_w are the air and water stresses on the ice, σ is the ice stress, g is the gravity acceleration, and η is the sea surface elevation. Quadratic drag laws are usually taken for the air and water stresses.

Compact drift ice is plastic material. The internal ice stress is here described by an elastic-plastic constitutive law (Pritchard, 1981), determined by four elements: yield curve flow rule, elastic response, and kinematic relationship. An isotropic model is assumed. The plastic yield curve $\phi = \phi(\sigma_I, \sigma_{II}, p^*)$, where σ_I and σ_{II} are two stress invariants and p^* is ice strength, is diamond shaped with zero yield stress for opening, $-p^*/2$ for pure shear, and $-p^*$ for spherical compression. The strength parameter p^* is given by (Rothrock, 1975; Pritchard, 1981)

$$p^* = c^* \int_o^{hmax} h^2 a(h)\, dh \qquad (4)$$

where c^* is a coefficient, h_{max} is the maximum ice thickness, and $a(h)$ is the fraction of ice participating in the redistribution process. An exact form for c^* is $c^* = 1/2 \times \rho_i(\rho_w-\rho_i)/\rho_w \times gk \times [1 + \mu'/\tan\phi' \times \rho_i/\rho_w \times (k-1)]$ where ρ_w is water density, μ is ice-ice friction coefficient, and ϕ' is the slope angle of ridge keels. An associated flow rule determines the plastic stretching $\boldsymbol{D}_p = \lambda \times \partial\phi/\partial\sigma$ where λ is a nonnegative scalar coefficient to keep the stress on the yield curve.

The stress satisfies an isotropic linear elastic response $\sigma = (M_1 - M_2)\mathbf{I}\ \mathrm{tr}\boldsymbol{e} + 2M_2\boldsymbol{e}$ where M_1 and M_2 are the bulk and shear moduli of ice and $\boldsymbol{e}$ is elastic strain. The elastic strain satisfies the kinematic relation $D\boldsymbol{e}/Dt - \boldsymbol{W}\boldsymbol{e} + \boldsymbol{e}\boldsymbol{W} = \boldsymbol{D} - \boldsymbol{D}_p$ where $\boldsymbol{D} = (\boldsymbol{L} + \boldsymbol{L}^T)/2$ is stretching, $\boldsymbol{W} = (\boldsymbol{L} - \boldsymbol{L}^T)/2$ is spin, and $\boldsymbol{L} = \nabla\boldsymbol{u}$ is the velocity gradient.

The model equations are solved in a 2D area $\Omega(\boldsymbol{r}, t)$ with boundary $L(\boldsymbol{r}, t) = L_1(\boldsymbol{r}, t) \cup L_2(\boldsymbol{r}, t) \cup L_3(\boldsymbol{r}, t)$ where L_1 is a free boundary (ice edge), L_2 is a rigid fixed boundary, and L_3 is rigid moving (forced) boundary. The boundary of $\Omega(\boldsymbol{r}, t)$ is unknown (because of L_1). The governing equations must be appended by boundary conditions.

At the free boundary the kinematic and dynamic conditions are, respectively,

$$L_1: \quad R_t + \boldsymbol{u}\nabla R = 0, \qquad (5a)$$

$$\sigma \cdot \mathbf{n} = 0 \qquad (5b)$$

where $R(\boldsymbol{r}, t) = 0$ is the equation of the free boundary and $\mathbf{n}$ is a unit outward vector to the boundary. Eq. (5a) describes the movement of the free boundary due to movement of boundary particles due to local and advective changes and Eq. (5b) states that the normal stress at the ice edge is zero. Along the rigid boundaries

$$L_2: \quad u_n = 0 \ \text{ if } \boldsymbol{u} \cdot \mathbf{n} > 0 \qquad (5c)$$

$$L_3: \quad u_n = u_b \qquad (5d)$$

where u_n is the ice velocity component normal to L_2 component and u_b is the velocity of the moving rigid boundary.

Finally, the system must include initial conditions:

$$\Omega(\boldsymbol{r}, 0) = \Omega_o(\boldsymbol{r}),\ G(\boldsymbol{r}, h, 0) = G_o(\boldsymbol{r}, h),\ \boldsymbol{u}(\boldsymbol{r}, 0) = 0 \qquad (6)$$

Eulerian-Lagrangian techniques seem more promising in sea ice dynamics, though there are only a few known examples of their use (e.g., Ovsienko, 1976; Pritchard et al., 1990; Flato, 1993). The approach developed here is based on particle-in-cells technique (PIC), but differs from the original one developed by Harlow (1964). A comprehensive description is beyond the scope of this paper and will be presented in a coming future publication. Some details of the scheme were presented in Ovsienko et al. (1995).

2.2 Ice Tank Experiments

The tank experiments are described in detail by Tuhkuri and Lensu (1997). In brief, the test region was of size 6 x 20 m (Fig. 2). The ice pack consisted of floes of a given thickness, size and shape. The ice was forced from one end by a boundary boom set to a fixed velocity u_b. The

initial compactness was 0.7. The only measured data are the force histories at the pusher plate. Several parameters were varied in the tank tests: ice thickness, pusher plate velocity, floe size and floe shape.

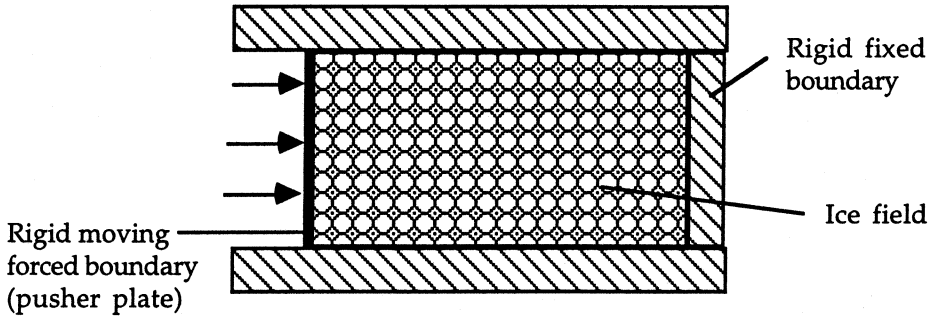

Fig. 2. The ice tank test design (Tuhkuri and Lensu, 1997). The size of the ice field is 6 x 20 m initially when the forcing begins.

For mathematical modeling of the tank test, the wind stress is zero and also the Coriolis force and the sea surface pressure gradient can be neglected. The ice is forced in one direction by the pusher plate at one boundary (Fig. 2). The equation of motion is then reduced into

$$m D\boldsymbol{u}/Dt = A\,\tau_w + \nabla\cdot\sigma \qquad (7)$$

The water stress is taken as a quadratic form $\tau_w = -\rho_w C_w |\boldsymbol{u}|\boldsymbol{u}$ where C_w is the ice-water drag coefficient. Due to the small scale of the experiments and rather low forcing speeds, the inertia and water drag terms are quite small.

3. RESULTS

3.1 Analytic Analysis

The ice tank problem can be examined analytically by a one-dimensional model (see Leppäranta, 1998). The inertia and water stress being small, the momentum equation (7) is further reduced to a quasi- steady form

$$\partial\sigma/\partial x = 0 \qquad (8)$$

The stress is constant in space and by the boundary condition it must correspond to the force F at the pusher plate: $\sigma = -F/b$ where b is the width of the ice field. On the other hand, under plastic compression the stress is equal to the yield strength σ_Y. In general, σ_Y depends on the ice thickness, and thus Eq. (8) tells that the ice thickness must also be independent on x. In the tank experiment, initially the ice thickness is h_o and the length of the ice field is l_o, and the conservation of volume requires that $hl = h_o l_o$ at any time. Thus

$$-F/b = \sigma_Y(h),\ h(t) = h_o l_o/(l_o - u_b t) \qquad (9)$$

In the tank test there is first a compaction phase where the compactness increases from the initial 0.7 to the maximum packing level. The 1D maximum packing is simply 1.0 which is reached at time $t = 0.3 l_o / u_b$. Then under further compression the floes start to ride up on each

other. Because ice thickness is constant in space, no individual ice ridge forms but instead the thickness increases uniformly all over in the ice field.

The elastic-plastic model given in chapter 2 has compressive yield strength of $-p^*$. For a constant ice thickness, the expression (3) integrates into $p^* = c^* h^2$, and the measured force history should read

$$F = b \times c^* h^2 = b \times c^* h_o^2 \times (1 - u_b t / l_o)^{-2} \qquad (10)$$

which is an increasing function of time approaching a sharp singularity at $t \rightarrow l_o/u_b$. For comparison, the viscous-plastic model of Hibler (1979) defines the compressive strength as $p^* = -P^* h \exp[-(1-A)C]$ where P^* and C are constants and A is ice compactness. The predicted force history would be rapidly increasing during the compaction phase and then as in Eq. (10) but with the powers of 1 for h_o and -1 for $(1 - u_b t / l_o)$.

3.2 Full Numerical Model

The objective of these preliminary calculations was not to exactly reproduce experiments in ice tank, but to adapt a large-scale ice model to laboratory experiment conditions and evaluate how it can be useful in understanding of such experimental results.

The model basin is of a rectangular shape with dimensions approximately the same as in the ice tank (6 x 20 m). In all simulations, at $t = 0$ the ice is at rest with compactness $A_o = 0.7$. Three boundaries are unmoved solid boundaries, and the left boundary starts to move in the x-axis direction at $t = 0$ with constant velocity. The parameters used in the numerical simulation are listed in Table 1. The ice-water drag coefficient is taken as 0.016 (Pritchard, 1990). The elastic moduli is constant, but large enough, limiting elastic strains to about 0.25-0.5 % of the total strain (Pritchard, 1981).

Table 1. The values of the parameters used in the numerical simulations. For the definition of the *b*-function, see Fig. 1.

Initial conditions		
Initial ice thickness	h_o	0.054 m
Initial ice compactness	A_o	0.7
Velocity of moving boundary	u_b	0.015, 0.033, 0.052
Model parameters		
Ice density	ρ	910 kg/m^3
Water density	ρ_w	1030 kg/m^3
Ice-water drag coefficient	C_w	0.016
Elastic modulus	M_1; M_2	2.0 MN/m^2; $M_1/2$
Ridging coefficient	k	6
b-function	G^*, G_o, G_1, B_o	0.55, 0.05, 0.2, 0.9
Sliding friction	μ	0.35
Ridge shape angle	ϕ'	10 deg

The study cases were here limited to the variations in ice thickness and pusher plate velocity because we cannot now take into account ice floe size and shape in the present model. Three test cases were chosen as the base for comparisons, characterized by uniform circular ice floes with some brash between, constant ice strength, and only the pusher plate velocity varied.

Since the dominant forces are here the pusher plate boundary force and the internal friction of the ice, we have good cases for evaluating the ice stress response to deformation. Though

pure ridge formation did not occur in these tests, for the ice strength evaluation we use potential energy changes and friction losses consistent with a ice ridge formation model (Rothrock, 1975). No difference is made between ridging and rafting except for the ratio of the potential energy to frictional losses in the redistribution process. The main tuning parameters are the ridging coefficient k (5-15), angle ϕ' describing ridge shape, and the shape of the function b. The ice-ice sliding friction coefficient μ is assumed constant as in Pritchard (1981). The force histories at the pusher plate can be used for the comparisons between the tank tests and the mathematical model. It is convenient to use a dimensionless time $t^* = u_b t/l_0$ where l_0 is the initial length if the ice field.

The first calculations with $\phi = 39°$ and $k = 5$ (as recommended by, e.g., Pritchard, 1981) resulted in underestimation of the force by about the factor of three; $k = 10$ gave the force curve far from the real shape. Without changing other parameters, the best choice turned out to be $k = 6$ and $\phi = 10°$ (Fig. 3). These values give the ratio of frictional losses to potential energy change equal to about 10. It is interesting that the relative thickness of ridged ice varied from 5.82 to 6.04 at the end of these experiments. The model curves for the different pusher plate velocities coincide almost completely, small differences are notable at the last stage possibly exhibiting inertia and water stress effects (Fig. 4). The experimental curves are also very similar in the dimensionless coordinates demonstrating rate-independent behavior. A slightly lower force in two tank tests was explained by the ice channel breaking in them (Tuhkuri and Lensu, 1997) but the difference is small and does not affect on the shape of the curves.

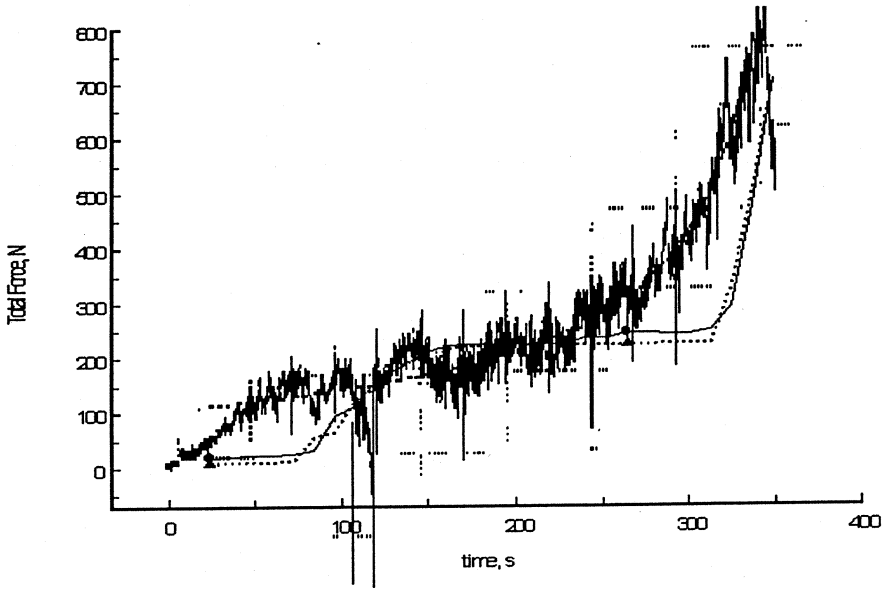

Fig. 3. The force at the pusher plate in the ice tank test (irregular line) compared with the model outcome at the pusher plate (solid line) and at the opposite wall (dotted line). Test #14 with pusher plate velocity u_b = 52 mm/s. The tank data are from Tuhkuri and Lensu (1997).

The force histories in the tank tests and mathematical model outcome differ much in the beginning and the end phases. This may be explained by the shape of the ridging participation function b, in particular by too small amount of ice available for ridging for $G > G_1$ and sharp transition in the slope of the curve at this point. The hypothesis about k being a constant seems also too primitive. The reason for the underestimation of the stresses may also be caused by

processes which do not affect on the ice thickness and therefore are not considered in the redistributor, e.g. friction along floe boundaries.

Ice thickness profiles plotted in dimensionless space coordinate $x^* = x/l$ where l is the position of the moving boundary are shown in Fig. 5 for different times. A weak dependency of the boundary velocity is seen.

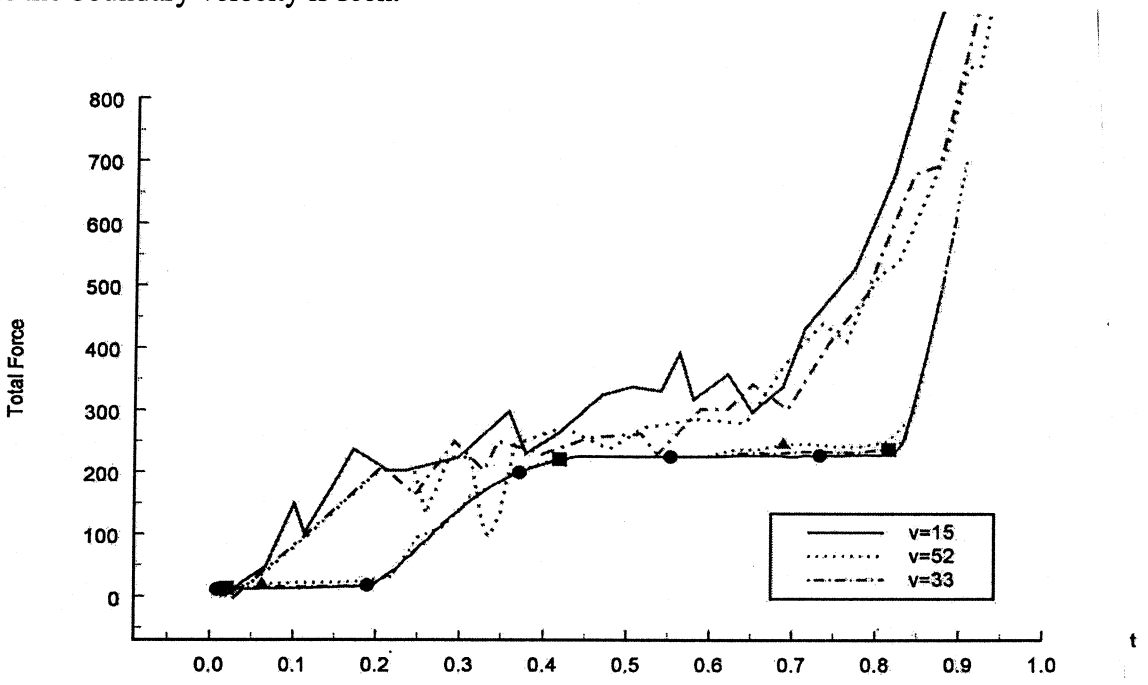

Fig.4. The force at the pusher plate as a function of dimensionless time (scaled by v/l_o), v is the pusher plate speed and l_o is initial ice field length. The model curves are with markers; the measured data are from Tuhkuri and Lensu (1997).

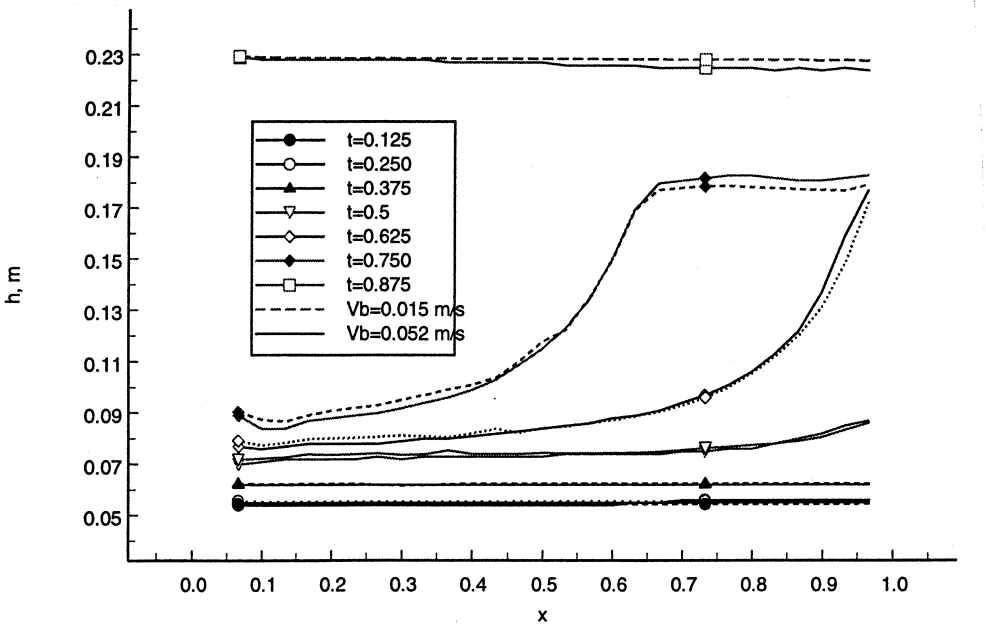

Fig. 5. Ice thickness profiles at different times t for pusher plate speeds v_b = 15 and 52 mm/s as resulted from the model.

4. CONCLUSIONS

Small scale ice tank experiments on ridging and rafting of granular ice have been examined using a continuum sea ice dynamics model designed for mesoscale modeling. The results are promising for the feasibility of ice tank tests to help understanding mesoscale sea ice dynamics.

The mathematical model reproduced reasonably well the principal measured quantity - the force at the moving boundary (pusher plate). Both the tank tests and the model outcome show rate-independent plastic behavior in wide range of velocities. In places the force was underestimated which was likely due to an inappropriate ridging function approximation.

This study is presently widened to include other ice rheologies to be tested. It will also be possible to examine the role of additional ice field properties such as the ice floe size and shape using the whole set of tank test series.

Acknowledgments. The work of M. Leppäranta was supported by the European Commission, DG XII, through the Marine Science and Technology Program, 1994-1998 (MAST III) under contract MAS3-CT95-0006 (ICE STATE). ICE STATE comprises Helsinki University of Technology, Nansen Environmental and Remote Sensing Center, Scott Polar Research Institute, University of Helsinki, and University of Iceland.

5. REFERENCES

Harlow F.H. 1964. The Particle-in-Cell Computing Method in Fluid Dynamics. *Methods Comput. Phys.* **3**, 319-343.

Hibler, W.D., III 1979. A dynamic thermodynamic sea ice model. *J. Phys. Oceanogr.* **9**, 815-846.

Flato, G.M. 1993. A particle-in-cell sea ice model. *Atmosphere-Ocean* **31**(3).

Leppäranta, M. 1998. The Dynamics of Sea Ice. In *Physics of Ice-Covered Seas*, Ed. M. Leppäranta, pp. 305-342. University of Helsinki Press, Helsinki.

Ovsienko, S. 1976. Numerical modeling of the drift of ice. *Izv., Atmospheric and Oceanic Physics* **12**(11), 1201-1206.

Ovsienko, S., Ivchenko, A. Zatsepa, S., Nechvolodov, L., Iakovlev, N., Pritchard, R., Driver, D. 1995. Kara Sea ice-ocean model. *Proc. 13th Internat. Conf. POAC*, Murmansk, Russia.

Pritchard R.S. 1981. Mechanical behavior of pack ice. *Mechanics of Structured Media*, Ed. by A.P.S. Selvadurai. pp. 369-405. Elsevier, Amsterdam.

Pritchard, R.S., Mueller, A.S., Hanzlick, D.J. and Yang, Y.-S. 1990. Forecasting ice edge motion in the Bering Sea. *J. Geophys. Res.* **95**(1), 775-788.

Rothrock, D.A. 1975. The energetics of the plastic deformation of pack ice by ridging. *J. Geophys. Res.* **80**, 4514-4519.

Thorndike, A.S., Rothrock, D.A., Maykut, G.A. and Colony, R. 1975. The thickness distribution of sea ice. *J. Geophys. Res.* **80**, 4501-4513.

Tuhkuri, J. and Lensu, M. 1997. Ice tank tests on rafting of a broken ice field. Report M-218, Helsinki University of Technology, Ship Laboratory.